PCCP

ROYAL SOCIETY OF CHEMISTRY

PAPER

View Article Online
View Journal | View Issue

Cite this: *Phys. Chem. Chem. Phys.*, 2026, **28**, 7101

A Zundel ion in the catalytic proton transfer pathway of [FeFe]-hydrogenase

Lingling Liu,[a] Max A. Klamke,[b] Federica Arrigoni,[c] Oliver Lampret,[a] Julian Kleinhaus,[d] Ulf-Peter Apfel,[de] Eckhard Hofmann,[f] Claudio Greco,[g] Thomas Happe,[a] Sven T. Stripp *[b] and Jifu Duan *[a]

[FeFe]-hydrogenases are metalloenzymes that catalyze the interconversion of protons, electrons, and molecular hydrogen (H_2). Their active site cofactor consists of a [4Fe-4S] cluster ($[4Fe]_H$) and a diiron site ($[2Fe]_H$), forming the so-called H-cluster. In this work, the putative regulatory proton transfer pathway (PTP) toward the $[4Fe]_H$ cluster of [FeFe]-hydrogenase *Cp*I from *Clostridium pasteurianum* is characterized by X-ray crystallography, infrared spectroscopy, and quantum mechanical (QM) calculations. The trajectory consists of asparagine N160, glutamine Q195, and several protein-bound water molecules that might function as a PTP toward cysteine C499 at the $[4Fe]_H$ cluster. We have hypothesized that protonation of C499 determines the H-cluster intermediate $H_{ox}H$ (M. Senger *et al.*, *Phys. Chem. Chem. Phys.*, 2018, 20, 3128–3140). The crystal structures of protein variants N160L and Q195L now confirm that the putative regulatory PTP is disrupted. However, infrared spectroscopy reveals that all variants accumulate the $H_{ox}H$ state in a manner comparable to wild-type *Cp*I. In contrast, the *Cp*I variant E279D – previously shown to target the catalytic PTP toward $[2Fe]_H$ – is found to enrich the $H_{ox}H$ state independently of reducing agents. This indicates that the determinants of $H_{ox}H$ are located in the catalytic PTP, which emphasizes the importance of $H_{ox}H$ during catalysis and provides evidence against any involvement of the putative regulatory PTP in hydrogen turnover. Supported by QM calculations, a model is proposed in which a conserved water cluster adjacent to E279 is protonated to form a Zundel ion ($H_5O_2^+$). Our results paint a new picture of the H-cluster in the $H_{ox}H$ state and yield important insight into the catalytic mechanism of [FeFe]-hydrogenases.

Received 5th November 2025,
Accepted 24th February 2026

DOI: 10.1039/d5cp04267d

rsc.li/pccp

Introduction

[FeFe]-hydrogenases are efficient H_2 catalysts with proton reduction rates exceeding 10 000 s^{-1}.[1,2] The active site cofactor (H-cluster) consists of a [4Fe-4S] cluster ($[4Fe]_H$), which serves as an electron relay, and an unique diiron site ($[2Fe]_H$) connected by a bridging cysteine thiol group.[3–5] A proximal iron ion (Fe_p) is distinguished from a distal iron ion (Fe_d). $[2Fe]_H$ contains an aminodithiolate ligand (adt), three carbonyl ligands (CO), and two cyanide ligands (CN^-).[6] The infrared (IR) absorbance bands of CO and CN^- are sensitive to changes of electron density in the first and second coordination sphere of the H-cluster,[7] which makes Fourier-transform infrared (FTIR) spectroscopy an ideal tool for investigating redox and protonation intermediates of the H-cluster *via* the Vibrational Stark Effect (VSE).[8,9] [FeFe]-hydrogenases have been investigated by FTIR spectroscopy in solution, in crystalized form,[10,11] and within living cells.[12]

The active-ready oxidized state H_{ox} with its $[4Fe\text{-}4S]_H^{2+}$-$[Fe_p^{II}Fe_d^{I}]_H$ configuration is generally considered to be the initial state of the catalytic cycle.[13,14] Other states include the one-electron reduced states $H_{red'}$ (also called H_{red}) or H_{red} (also called $H_{red}H^+$), which are distinguished by reduction either at $[4Fe]_H$ or $[2Fe]_H$. Additionally, the two-electron reduced states $H_{sred}H^+$ ($[4Fe]_H^+$-$[Fe_p^{I}Fe_d^{I}]_H$, also called H_{sred}) and H_{hyd} ($[4Fe]_H^+$-$[Fe_p^{II}Fe_d^{II}]_H$) have been described.[15–19] A five-step catalytic cycle involving all of these intermediates was proposed.[20–22] We will

[a] *Photobiotechnology, Faculty of Biology and Biotechnology, Ruhr University Bochum, Universitätsstrasse 150, 44801 Bochum, Germany. E-mail: jifu.duan@ruhr-uni-bochum.de*
[b] *Spectroscopy & Biocatalysis, Institute of Chemistry, University of Potsdam, Karl-Liebknecht- Straße 24-25, 14476 Potsdam, Germany. E-mail: sven.stripp@uni-potsdam.de*
[c] *Department of Biotechnology and Biosciences, University of Milano-Bicocca, Piazza della Scienza 2, 20126, Milan, Italy*
[d] *Inorganic Chemistry I, Faculty of Chemistry and Biochemistry, Ruhr University Bochum, Universitätsstrasse 150, 44801 Bochum, Germany*
[e] *Department of Energy, Electrosynthesis Group, Fraunhofer UMSICHT, 46047 Oberhausen, Germany*
[f] *Protein Crystallography, Faculty of Biology and Biotechnology, Ruhr University Bochum, Universitätsstrasse 150, 44801 Bochum, Germany*
[g] *Department of Earth and Environmental Sciences, University of Milano-Bicocca, Piazza della Scienza 1, 20126 Milan, Italy*

Table 1 FTIR signature and electronic configuration of *Cp*I H-cluster intermediates with a mixed-valence, oxidized $[2Fe]_H$ cluster. Data for H_{ox} and $H_{ox}H$ as published,[24] data for $H_{red'}$ and $H_{red'}H$ presented in this study (Fig. S1)

Redox species	νCN^- (cm^{-1})	νCO (cm^{-1})	$[4Fe]_H$ charge	Fe_p/Fe_d charge	Charge difference
H_{ox}	2081, 2068	1970, 1947, 1801	+2	II/I	—
$H_{ox}H$	2084, 2074	1975, 1953, 1808	+2	II/I	—
$H_{red'}$	2075, 2064	1961, 1938, 1788	+1	II/I	1
$H_{red'}H$	2078, 2071	1971, 1944, 1803	+1	II/I	1

address the catalytic mechanism in the Discussion section (*vide supra*).

In previous work, we reported an additional H-cluster intermediate that accumulated at acidic pH and in the presence of sodium dithionite (NaDT, an artificial electron donor for H_2 production) and assigned it to a protonated oxidized state, $H_{ox}H$.[23–25] The FTIR spectra of H_{ox} and $H_{ox}H$ differ by a small upshift of all cofactor bands (Table 1). Density functional theory (DFT) calculations supported that $H_{ox}H$ harbors an additional proton at a cysteine ligand of $[4Fe]_H$ (*i.e.*, C499 in *Cp*I) that is not present in the H_{ox} state.[24] Small differences between the EPR spectra of H_{ox} and $H_{ox}H$ are in agreement with this interpretation.[25] A protonation of $[4Fe]_H$ was discussed in other intermediates as well and might play a role in stabilizing the reduced $[4Fe]_H$ cluster in $H_{red'}$, which would facilitate a direct transition into H_{hyd}.[26] In fact, H_{hyd} can be enriched in wild-type [FeFe]-hydrogenase directly *via* $H_{ox}H$ upon H_2 oxidation.[17] At higher driving force, H_{hyd} accumulates under alkaline conditions, too.[27] The discovery of $H_{ox}H$ inspired a novel three-step catalytic cycle that only contains H_{ox} ($H_{ox}H$), $H_{red'}$, and H_{hyd} and allowed circumventing the $[2Fe]_H$-reduced states $H_{red}H^+$ and $H_{sred}H^+$ (*vide supra*).[20–22] Although it has been shown that $H_{ox}H$ may form upon contact with sulfite as a degradation product of NaDT, the conversion of H_{ox} into $H_{ox}H$ in the presence of reductants like TCEP, DTT, ascorbic acid, or Eu(II)-ETPA confirmed that $H_{ox}H$ is not a side-product of sulfite inhibition.[28–30] However, direct evidence for a protonated cysteine ligand has not been obtained. So far, there is no consensus regarding the nature of $H_{ox}H$ and its impact on the catalytic cycle.

Proton transfer in the [FeFe]-hydrogenase from *Clostridium pasteurianum Cp*I is facilitated by a catalytic proton transfer pathway (PTP) comprised of several conserved amino acid side chains and protein-bound water molecules, *i.e.,* C299, water molecules W1 and W2, E279, S319, E282, and R286 (Fig. 1).[31–34] While it might be reasonable to speculate that the protonation leading to $H_{ox}H$ occurs through the catalytic PTP, this possibility was excluded because of the observation that the proton transfer-incompetent amino acid variant *Cp*I-C299A accumulated $H_{ox}H$ just like wild-type protein.[17,24] The same is true for semi-artificial "cofactor variants" with non-polar ligands like propane or ethane dithiolate (pdt, edt), which allows excluding a protonated adt ligand in $H_{ox}H$.[24] Based on a comparison of various crystal structures of [FeFe]-hydrogenases from *C. pasteurianum* and *Desulfovibrio desulfuricans*, a "regulatory" PTP toward $[4Fe]_H$ was proposed comprising four consecutive water molecules W1′–W4′ that could transfer protons between C499 and bulk solvent (Fig. 1).[24]

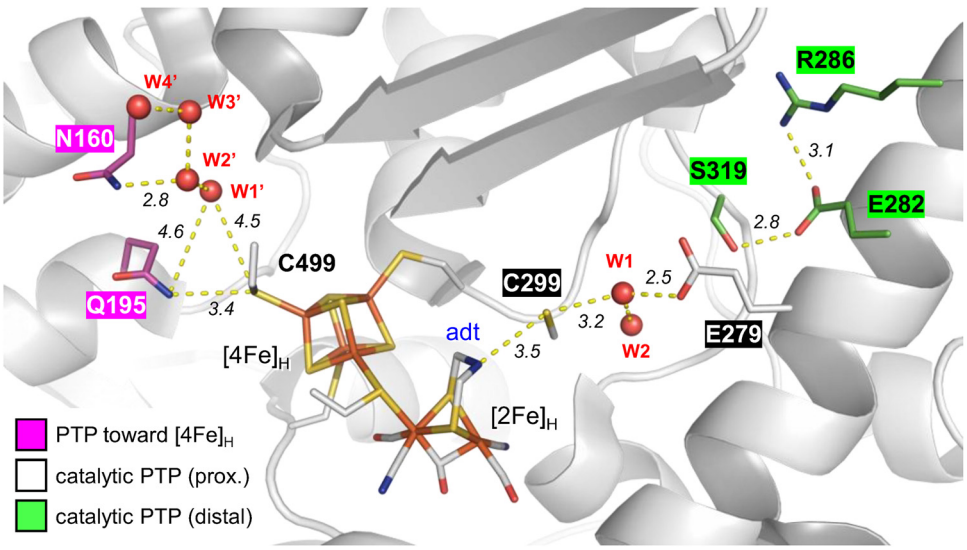

Fig. 1 The catalytic and putative regulatory proton transfer pathway (PTP) of [FeFe]-hydrogenase *Cp*I in the oxidized state. The catalytic PTP includes C299, water molecules W1/W2, and E279 in the trajectory proximal to the H-cluster (black labels) as well as S319, E282, and R286 in the distal section (green labels). The putative regulatory PTP is comprised of water molecules W1′–W4′. Polar amino acids N160 and Q195 (magenta labels) establish interactions with the water channel. Red spheres represent water molecules. Dashed yellow lines refer to H-bonds, and their distances are given in Å. The PDB ID is 4XDC.[5]

In *Cp*I, asparagine N160 and glutamine Q195 coordinate the water molecules that form the regulatory PTP toward cysteine C499 at the $[4Fe]_H$ cluster (Fig. 1). While only Q195 is strictly conserved in [FeFe]-hydrogenase, N160 has been shown to be linked to the O_2 sensitivity of *Cp*I.[35] In this work, we characterize the influence of the putative regulatory PTP *via* site-directed mutagenesis and pH-dependent *in vitro* assays, X-ray crystallography, FTIR spectroscopy, and DFT calculations. We find that the catalytic PTP must not be excluded when understanding the formation of $H_{ox}H$ after possible protonation sites in both *Cp*I and HydA1 from *Chlamydomonas reinhardtii* were studied. Our data support earlier speculations about a Zundel ion in the PTP and emphasize the significance of $H_{ox}H$ in the catalytic cycle of [FeFe]-hydrogenase.[31]

Results

$H_{ox}H$ is present in variants targeting the putative regulatory PTP

To investigate the possibility of proton transfer between C499 and bulk solvent *via* the putative regulatory PTP, site-directed mutagenesis was used to replace N160 and Q195 by the hydrophobic amino acid leucine with the aim of disrupting the water-based PTP and abolish proton transfer (Table S1). In H_2 evolution assays, we found that the activities of *Cp*I-N160L, *Cp*I-Q195L, and double variant *Cp*I-N160L-Q195L were not significantly different to wild-type *Cp*I (Fig. 2a) and exhibited an overall similar pH-dependency (Fig. S2). No shift in pH-optimum or drastically decreased H_2 evolution activity was observed, in marked difference to variants of the catalytic PTP as reported previously.[31] We evaluated the H_2 oxidation activities by means of protein film electrochemistry next. The activity of *Cp*I-N160L was not significantly different to wild-type *Cp*I, whereas *Cp*I-Q195L and *Cp*I-N160L-Q195L displayed lower H_2 oxidation activities toward acidic pH values (Fig. 2b). Analysis of the electrochemical data suggests slower catalysis and higher overpotentials for *Cp*I-Q195L and *Cp*I-N160L-Q195L (Fig. S3).

X-ray crystallography was then employed to determine changes in structures after mutagenesis. Variants were crystalized in the same space group as wild-type *Cp*I ($P12_11$) comprising two chains (A and B) in the asymmetric unit.[5,31] The structures of *Cp*I-N160L, *Cp*I-Q195L, and *Cp*I-N160L-Q195L were refined to resolutions at 1.45, 1.75, and 1.67 Å, respectively (Table S2–S4). The overall structures of these three variants superimposed with the structure of wild-type *Cp*I are presented in Fig. S4a, which shows that the substitutions did not change the general fold (Table S2). Local structural features of the putative regulatory PTP in double variant *Cp*I-N160L-Q195L and each single variant are presented in Fig. 3a and Fig. S4, respectively. The electron density of W1′, which is the closest water molecule to C499, is absent in variants *Cp*I-N160L-Q195L and *Cp*I-Q195L. Most likely, the disappearance of W1′ results from the removal of the polar glutamine side chain and the introduction of the hydrophobic leucine residue on position 195. In addition, W2′ shifted 0.5 Å away from L160 in *Cp*I-N160L-Q195L, likely resulting from the substitution of asparagine against leucine on position 160. This

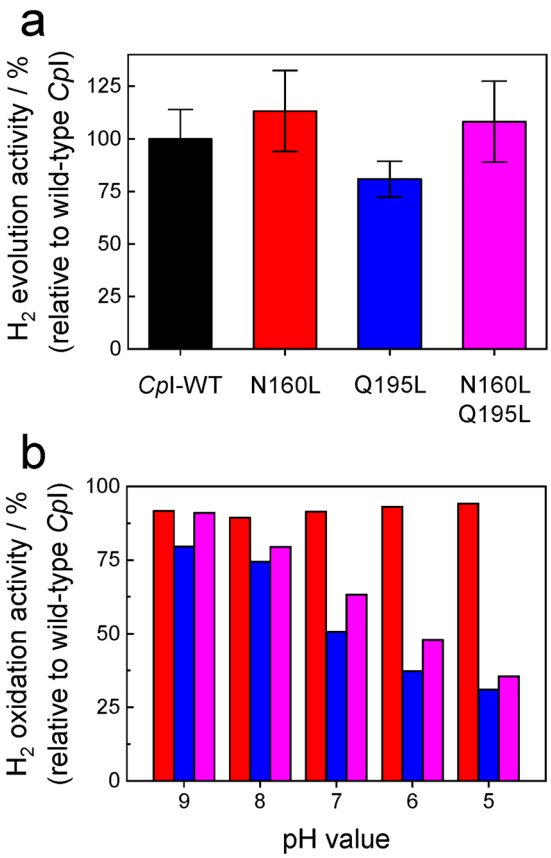

Fig. 2 H_2 evolution and H_2 oxidation activities. (a) Relative to wild-type *Cp*I, H_2 evolution activities for *Cp*I-N160L, *Cp*I-Q195L, and *Cp*I-N160L-Q195L (Fig. S2) are shown as an average across pH 5–9. Within the variation of the solution-based activity assay and gas chromatographic analysis none of the observed differences are significant. (b) Based on this observation, cyclic voltammograms (Fig. S3) were normalized at reducing potentials to compare the current at oxidizing potentials, the latter which is given here relative to wild-type *Cp*I. Note the stepwise decrease of H_2 oxidation activities for *Cp*I-Q195L (blue bars) and *Cp*I-N160L-Q195L (magenta bars) toward acidic pH values.

disrupts the original H-bonding network of the putative regulatory PTP. Therefore, *Cp*I-N160L-Q195L doubly guarantees the interruption of this PTP.

Subsequently, *Cp*I protein variants targeting the putative regulatory PTP were used to examine the influence of mutagenesis on the accumulation of $H_{ox}H$ *via* attenuated total reflection (ATR) FTIR spectroscopy. Infrared spectra of variants and wild-type *Cp*I prepared in NaDT-free buffer at pH 8 are shown in Fig. 3b. Under a N_2 atmosphere, both wild-type *Cp*I and *Cp*I-N160L-Q195L yielded almost pure H_{ox} state (grey shading). Titrating the protein films with fresh pH 4 buffer containing 10 mM NaDT, both wild-type *Cp*I and *Cp*I-N160L-Q195L fully converted into the $H_{ox}H$ state (blue shading). Similar results were obtained for *Cp*I-N160L and *Cp*I-Q195L (Fig. S5). At pH 4 but in the absence of NaDT, *Cp*I-N160L-Q195L showed the same spectrum of wild-type *Cp*I, *i.e.*, only H_{ox} was formed (Fig. S5, Fig. 4a and Table S5). These observations highlight the similarities of double variant and wild-type *Cp*I. The accumulation of $H_{ox}H$ in the variants challenges previous

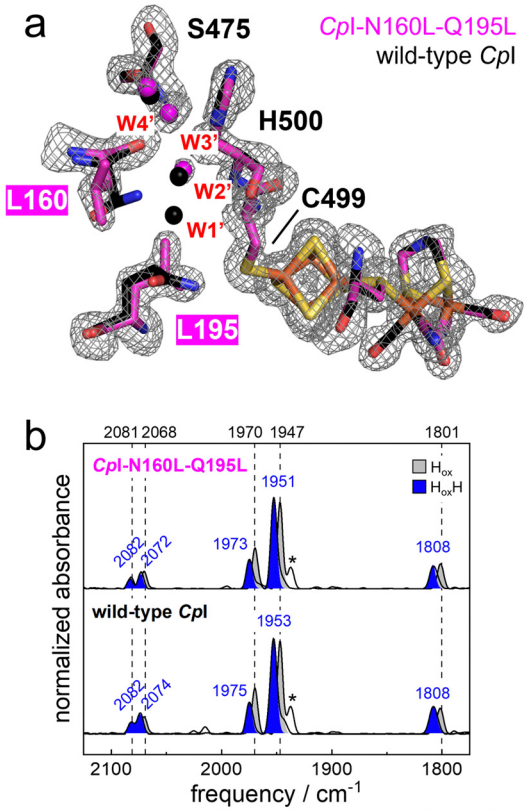

Fig. 3 Structural features of double variant *Cp*I-N160L-Q195L and FTIR spectra. (a) The electron density map of *Cp*I-N160L-Q195L (stick model, PDB ID 9RJO, chain B) is superimposed with wild-type *Cp*I (WT, PDB ID 4XDC, chain B). W1′ of wild-type *Cp*I vanished in *Cp*I-N160L-Q195L. Simulated annealing omit-map ($F_o - F_c$) was contoured at 2σ. For wild-type *Cp*I and *Cp*I-N160L-Q195L, carbon atoms and water molecules are colored black and magenta, respectively. (b) At pH 8, the H_{ox} state (grey shading and dashed lines) is enriched under N_2 in both wild-type *Cp*I and *Cp*I-N160L-Q195L. The asterisk (*) indicates a small fraction of H_{red}'. At pH 4 and in the presence of 10 mM NaDT, the up-shifted $H_{ox}H$ state (blue shading) can be observed in both wild-type *Cp*I and *Cp*I-N160L-Q195L.

speculations about protonation on $[4Fe]_H$ through the putative regulatory PTP.

The catalytic PTP affects the formation of $H_{ox}H$

When revisiting our previous work,[31] we realized that FTIR spectra of different variants targeting the catalytic PTP in *Cp*I (Fig. 1) showed difference in the enrichment of H_{ox} and $H_{ox}H$ at alkaline pH and in the presence of 2 mM NaDT. For example, *Cp*I variants C299A, E279D, and E282D contained approximately 80%, 45%, and 30% $H_{ox}H$, which implies a potential correlation between the catalytic PTP and the formation of $H_{ox}H$. Thus, these variants and the corresponding sites in the [FeFe]-hydrogenase from *Chlamydomonas reinhardtii* (*Cr*HydA1 C169D, E141D, S189A, and E144D) were re-examined systematically.

The experiments were carried out in NaDT-free buffer at pH 8, NaDT-free buffer at pH 4, or 10 mM NaDT at pH 4. All buffers containing NaDT were prepared fresh as dithionite salts are not stable in aqueous solution.[36] Before the variants were measured, wild-type *Cp*I and *Cr*HydA1 were probed by ATR FTIR spectroscopy as shown in Fig. 4a and Fig. S6, respectively. At pH 8 and in the absence of NaDT, H_{ox} accumulated under N_2 purging. When NaDT-free buffer at pH 4 was titrated onto the protein films, no changes could be observed and H_{ox} remained. In contrast, titrating the protein films with 10 mM NaDT in buffer at pH 4 caused a clear up-shift of the oxidized state, *i.e.*, a conversion of H_{ox} into $H_{ox}H$. These results are fully consistent with earlier observations, emphasizing the importance of both acidic pH and reducing agents on the formation of $H_{ox}H$.[21,23,24,28,29] Following the same protocol, *Cp*I-C299D/*Cr*HydA1-C169D, *Cr*HydA1-S189A, and *Cp*I-E282D/*Cr*HydA1-E144D exhibited a similar behavior, *i.e.*, no conversion from H_{ox} into $H_{ox}H$ unless both acidic and reducing conditions were present (Fig. S7). Analogous to wild-type protein, variants targeting the catalytic PTP showed little influence on the formation of the $H_{ox}H$ state.

Interestingly, one variant behaved differently. When *Cp*I-E279D was prepared in NaDT-free buffer at pH 8 and analyzed by FTIR spectroscopy, a pattern including bands in 1797, 1943,

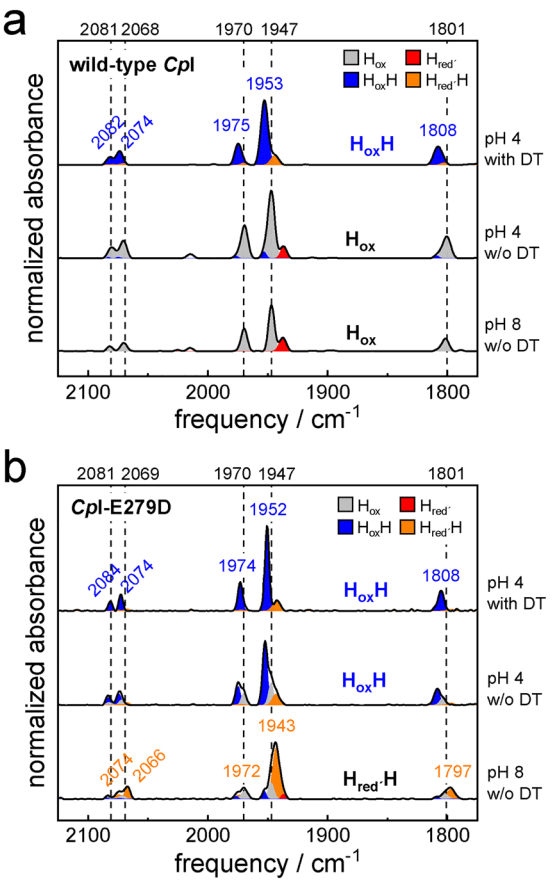

Fig. 4 FTIR spectra of wild-type *Cp*I and *Cp*I-E279D at different conditions. (a) Wild-type enzyme adopted the $H_{ox}H$ state only under acidic conditions (pH 4) and in the presence of sodium dithionite (NaDT). (b) In variance, PTP variant *Cp*I-E279D accumulated the $H_{ox}H$ state under acidic conditions already in the absence of reductant. Colors refer to fits of experimental data (H_{ox}, grey; $H_{ox}H$, blue; H_{red}', red; $H_{red}'H$, orange).

1972, 2066, and 2074 cm^{-1} was observed (Fig. 4b). Compared to wild-type *Cp*I, this suggests a down-shifted H_{ox} state roughly similar to $H_{red'}$ (Table 1); however, the mean CO/CN^- frequency falls right between these two intermediates (Fig. S1), which is why we assign the signature to the $H_{red'}H$ state as characterized previously.[24] We assume that *Cp*I-E279D was in contact with the reducing atmosphere of the glovebox (1–2% H_2) and accumulated the $H_{red'}H$ state due to H_2 oxidation. The corresponding *Cr*HydA1-E141D variant (*vide supra*) does not show this state. After titrating the *Cp*I-E279D protein film with NaDT-free buffer at pH 4, peaks at 1808, 1953, 1975, 2074, and 2084 cm^{-1} were observed, which precisely matches the band pattern of $H_{ox}H$.[23,24] Notably, we strictly excluded NaDT in this titration and protein preparation; when NaDT was included at pH 4, *Cp*I-E279D fully converted into the $H_{ox}H$ state analogous to wild-type *Cp*I and the other PTP variants. To rule out the possibility that diluted proteins films provide an insufficiently high pH – which would prevent the accumulation of the $H_{ox}H$ state in wild-type *Cp*I – we plotted spectra of the H-cluster during the dehydrating process. The latter affects the protein concentration that can be followed *via* the amide II band between 1535–1540 cm^{-1} (Fig. S8). In the case of wild-type *Cp*I, the H_{ox} state did not convert into $H_{ox}H$ at all; however, significant conversion from H_{ox} to $H_{ox}H$ is monitored after the *Cp*I-E279D protein film was carefully dehydrated. These results were reproducible in the corresponding variant *Cr*HydA1-E141D (Fig. S9). Surprisingly, our data now demonstrate that the presence of NaDT is not an essential precondition for accumulating $H_{ox}H$ in this variant, and that substitutions at E279 (*Cp*I) or E141 (*Cr*HydA1) of the catalytic PTP indeed affect the formation of the $H_{ox}H$ state. The importance of this observation is emphasized by data that show how *Cr*HydA1-E141D converts into H_{hyd} upon reduction by H_2, notably in the absence of NaDT (Fig. S9).

Calculating the spectral differences between H_{ox} and $H_{ox}H$

To gain further insight into the nature of the $H_{ox}H$ state we carried out DFT calculations using a QM-cluster approach, based on an H-cluster model encompassing a portion of the catalytic PTP (Fig. S11). Specifically, we considered a set of representative structures to investigate how different proton arrangements and protonation states within the PTP may affect the H-cluster's IR signature (Fig. 5 and Fig. S12). Three main variables were explored: (i) the orientation of the N–H group of the adt bridgehead nitrogen (and consequently the position of the C299 thiol within the H-bond network), (ii) the protonation state of residue E279 (either anionic or neutral), and (iii) the addition of an additional proton near W1, potentially leading to the formation of a Zundel ion involving W1 and W2.[37]

The two adt N–H bond orientations (Fig. 5 and Fig. S12) were included to assess whether this structural detail could influence the spectroscopic outcome, although it is well established – and confirmed by our calculations – that the configuration in which the N–H points toward Fe_d is thermodynamically more stable by approximately 6–10 kcal mol^{-1}, depending on the protonation state considered. When starting from a deprotonated E279 (A1 in Fig. 5), the addition of a proton near W1 and W2 does not result in Zundel ion formation; instead, E279 is spontaneously protonated (A2). This behavior is fully consistent with the unusually high pK_a ($\sim$8.6) previously proposed for this residue,[31] which facilitated its FTIR characterization under physiological condition.[38] Assuming E279 as neutral (A2 in Fig. 5), the addition of one proton leads to the formation of a Zundel ion between the two water molecules, stabilized by a hydrogen-bond network involving E279, C299, and K322 (A3).

Overall, the IR spectrum calculated for H_{ox} based on model A2 shows satisfactory agreement with the experimental data, faithfully reproducing the observed frequencies with unsigned errors ranging within 4–27 cm^{-1}. The only exception is the band associated with Fe_d–CN^- that systematically deviates by a significantly larger extent, the unsigned error being 70 cm^{-1} with respect to the experimental value, notably across all calculations and irrespective of the functional used. We assume that this discrepancy arises from the fact that Fe_d–CN^- and K358 can form a salt bridge[3] that is not screened by the protein matrix in our model, or even by an implicit dielectric (see the

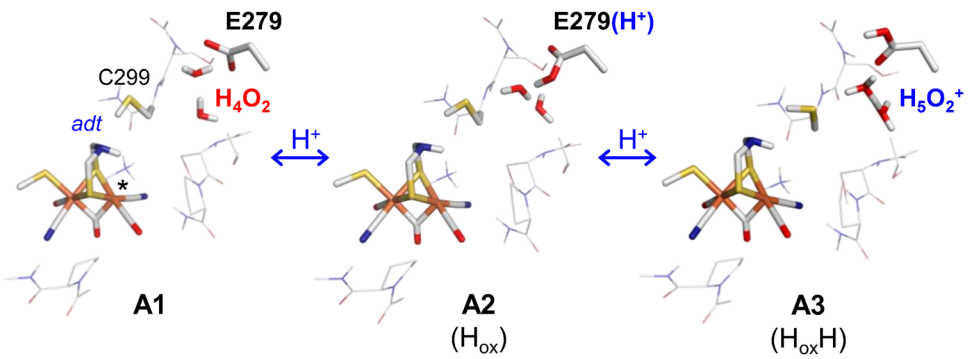

Fig. 5 Optimized structure obtained by progressively adding one proton starting from an H_{ox} model with hypothetical deprotonated E279. In configuration A1, the N–H group of the adt ligand points toward Fe_d (*) and C299 interacts with the lone pair of the adt nitrogen. Configuration A2 features a protonated E279 residue, which is the most likely configuration at pH 7. Therefore, structure A2 will be used as reference for H_{ox}, to which a second proton can be added to form a Zundel ion ($H_2O_5^+$). The Zundel ion in structure A3 is stabilized through multiple H-bonds, involving E279 and the side chain of C299, as well as the backbone of C299 and K322. The additional proton is shared between the two oxygen atoms of W1 and W2.

Experimental section related to DFT calculations for details). This deviation is negligible for the type of analysis conducted in this study and does not affect the reliability of our conclusions. Our focus is on the shift of IR bands upon protonation (or proton rearrangement), and cancellation of errors are expected when shifts are computed based on DFT data. Moreover, the experimentally observed CO band shifts are more pronounced and more sensitive and therefore particularly suitable for theory-experiment comparisons.

Notably, a clear upshift of the IR bands is observed when comparing the spectra of H_{ox} before and after proton addition (*i.e.*, before and after Zundel ion formation, ΔA3/A2 in Fig. 5), consistent with the experimental differences between H_{ox} to $H_{ox}H$. The computed shifts range from approximately 2–20 cm^{-1} and best match the experimental extent in models where the adt N–H bond is oriented toward Fe_d (Fig. S13). When using hybrid functionals, we find that the band associated with Fe_d–CN^-, which is generally the least well-reproduced, appears slightly down-shifted. Nevertheless, the overall trend remains robust across different theoretical levels, supporting the idea that proton accumulation in the catalytic PTP drives the observed spectral changes, irrespective of the specific H-bonding pattern.

Discussion

The putative regulatory PTP is comprised of a water chain held in place by the polar residues of amino acids N160 and Q195, the latter which is strictly conserved in [FeFe]-hydrogenases. The distance of 2.5–2.9 Å between the water molecules allows for strong H-bonding interactions and thus effective proton transfer.[39,40] However, the proximal water molecule (W1′) is 4.5 Å away from C499 at $[4Fe]_H$, which exceeds the optimal distance for H-bond formation (Fig. 1).[40,41] We speculate that the side chain of Q195 could play a role in donating protons to C499, which seems to be the only possibility for proton transfer toward $[4Fe]_H$ and the H-cluster. In PTP variant *Cp*I-N160L-Q195L, the large distance of 5.7 Å between W2′ and C499 illustrates that the trajectory has been severely disrupted (Fig. S14). The accumulation of $H_{ox}H$ in variants targeting the putative regulatory PTP is now in conflict with our earlier suggestion that protonation at C499 determines the $H_{ox}H$ state.[24] Although the variants are unaffected in their H_2 evolution activity, Q195 and the pool of water molecules at the backend of the H-cluster have an effect on the H_2 oxidation rates, in particular under acidic conditions (Fig. 2). The following reasoning can explain this observation. Ensing *et al.* argued that during electron transfer *via* the [4Fe-4S] relay chain, solvent water may penetrate into the vicinity of electron-accepting [4Fe-4S] clusters, probably in order to form a H-bonding network that stabilizes the redox states of the [4Fe-4S] clusters.[42] This would be in agreement with the experimentally observed redox anti-cooperativity between $[4Fe]_H$ and the [4Fe-4S] relay chain.[21] We speculate that the water molecules between the proximal [4Fe-4S] cluster and $[4Fe]_H$ may play a role in redox stabilization (Fig. S14). Such effects become obvious for variants *Cp*I-Q195L and *Cp*I-N160L-Q195L when carefully analyzing the respective voltammograms and their first derivative (Fig. S3). Here, the disruptions in the hydrogen-bonding environment may influence the reduction potential of the $[4Fe]_H$ site, which is evident from the increase of the required overpotentials and the significant shift of E^0 to more negative potentials, especially at low pH. Hence, a fine-tuned network of H-bonds along the [4Fe-4S] relay chain may guarantee an energetically favorable electron transfer route, which can be particularly important in the presence of H_2 and at low pH when [FeFe]-hydrogenase tend to accumulate the H_{hyd} state with its reduced $[4Fe]_H$ cluster.[17] However, an influence on the formation of $H_{ox}H$ must be excluded.

The NaDT-independent accumulation of $H_{ox}H$ in *Cp*I-E279D and *Cr*HydA1-E141D challenges former conclusions on the innocence of the catalytic PTP in forming the $H_{ox}H$ state.[24] In fact, our data imply now that the formation of $H_{ox}H$ is very likely to be dependent on the catalytic PTP, where a protonation at W1/W2 is responsible for the formation of the $H_{ox}H$ state. A dedicated regulatory PTP does not exist in [FeFe]-hydrogenase.

Comparing the crystal structures of wild-type *Cp*I (PDB ID 4XDC) and *Cp*I-E279D (PDB ID 6YF4),[5,43] significant differences around glutamic acid residue E279 are found (Fig. 6). In wild-type *Cp*I, the large distance of 3.8 Å between E279 and S319 presumably divides the catalytic PTP into two parts as proton transfer needs to overcome a high energy barrier.[11,38] It was also proposed that upon reduction of the H-cluster, the favored H-bond between E279 and W1 was weakened, and stronger interactions between E279 and S319 were formed, prompting direct proton transfer between E279 and S319. Therefore, proton transfer might be triggered by changes of the H-bond network involving E279, S319, and W1.[11,38] In wild-type *Cp*I, we propose that the high energy barrier resulting from a large distance of 3.8 Å between E279 and S319 restricts proton transfer onto W1 when NaDT or any other reductant is absent, even at low pH.[29] This is rationalized by concerted proton-coupled electron transfer (PCET) where the probability of proton tunneling across the catalytic PTP is significantly enhanced when coupled to redox chemistry at the H-cluster, even across larger distances.[43–46] Therefore, W1 remains unprotonated at low pH without NaDT in wild-type *Cp*I. Once a reductant is added – *e.g.*, NaDT, DTT, TCEP, or ascorbic acid[29] – PCET decreases the free-energy requirement for driving electrons and protons toward the active site,[43,45] so that the large gap between E279 and S319 is overcome with a physiologically relevant probability. As a result, W1 becomes protonated and forms a Zundel ion with W2, which causes the up-shift of H_{ox} and explains the accumulation of $H_{ox}H$. Please note that the water cluster in the crystal structure of *Cp*I-E279D does not suggest a Zundel ion;[47] at the given resolution of 1.6–1.8 Å, the O–O distance is only insignificantly different to wild-type enzyme.[5,43] The structure of *Cp*I-E279D likely represents H_{ox}. High resolution crystal structures with a dedicated accumulation of $H_{ox}H$ (and *in crystallo* FTIR characterization) may help identifying the Zundel ion.[11,48] Moreover, neutron diffraction

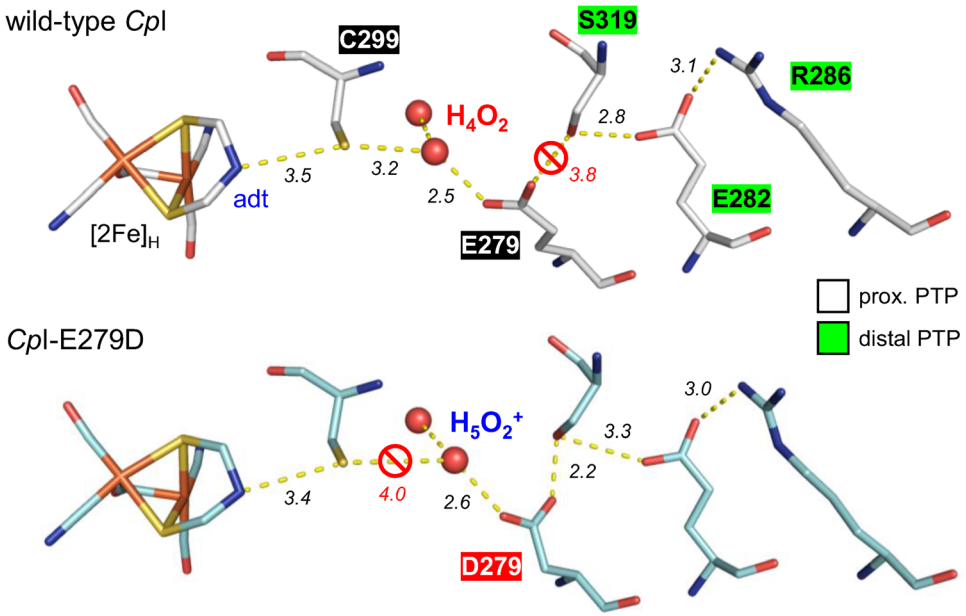

Fig. 6 Differences in the catalytic PTP between wild-type *Cp*I and *Cp*I-E279D. Distances between adjacent atoms within the PTP are shown in Å. The dashed lines indicate possible H-bonding interactions. Significant proton transfer barriers (> 3.5 Å, shown as "no access" signs) between E279–S319 and C299-W1/W2 were identified in wild-type *Cp*I (PDB ID 4XDC) and E279D (PDB ID 6YF4), respectively.

or cryogenic electron microscopy may facilitate a direct detection of the supernumerous proton in the future.[49,50]

Interestingly, W1 is about 0.8 Å further away from C299 in *Cp*I-E279D than in wild-type *Cp*I (3.2 *vs.* 4.0 Å, Fig. 6). This basically impairs any H-bonding interactions with C299. However, the carboxylic side chain in E279D is much closer to S319, which reduces the distance from 3.8 to 2.2 Å, compared to wild-type *Cp*I. The short distance allows for immediate proton transfer between E279 and S319. In this scenario, W1 becomes protonated without the need of concerted PCET, *i.e.*, even in the absence of NaDT. We assume that the Zundel ion is stable because C299 as the next H-bonding partner in *Cp*I-E279D is more than 4 Å away (Fig. 6) and proton transfer is inhibited unless additional driving force is applied. Therefore, protonation of W1/W2 causes an accumulation of $H_{ox}H$ in PTP variant *Cp*I-E279D without reductants. Please note that the final pH of the *Cp*I-E279D protein film was ill-defined at the time of measurement since the sample was prepared at pH 8 originally and then supplemented with one equivalent of pH 4 buffer. The structures of wild-type *Cp*I and *Cp*I-E279D in Fig. 6 were obtained at approximately pH 7.[5,43] The low pH structure of wild-type *Cp*I from Artz *et al.* was crystalized at pH 4.6 (PDB ID 6NAC) being more than 100x more acidic than the structure of wild-type *Cp*I (PDB ID 4XDC) as discussed here;[51] however, it shows nearly no difference in the distance of each adjacent functional group along the catalytic PTP, demonstrating that pH effects on the conformation of the PTP region in wild-type proteins seem to be insignificant.

Neither *Cp*I-E282D/*Cr*HydA1-E144D, *Cr*HydA1-S189A, nor *Cp*I-C299D/*Cr*HydA1-C169D accumulate $H_{ox}H$ in the absence of NaDT (Fig. S7). Structure analysis shows high similarities with wild-type *Cp*I in the region of E279 and S319 (Fig. S15). Accordingly, W1 is difficult to protonate at low pH alone in these variants. In the presence of NaDT, however, the protonation of W1 is facilitated by concerted PCET, thereby forming $H_{ox}H$ similar to wild-type *Cp*I.

The catalytic cycle involving a Zundel ion

We gathered evidence from structural biology, biochemistry, and spectroscopy that the $H_{ox}H$ state comprises a protonated water species in the catalytic PTP instead of a protonated $[4Fe]_H$ cluster. During catalysis, the H-cluster undergoes protonation events at the $[2Fe]_H$ cluster exclusively. Here, a reaction mechanism with changes in the catalytic PTP is proposed (Fig. 7). When triggered by high proton pressure (low pH), the water cluster becomes protonated and $H_{ox}H$ is populated over H_{ox}. One electron reduction yields $[4Fe]_H^+$ while W1/W2 is still protonated, which constitutes the $H_{red'}H$ state. Accumulation of the latter may alternatively proceed *via* reduction first ($H_{red'}$) and protonation second, or concerted PCET. Experimentally, this interdependency results in an apparent band broadening due to the simultaneous presence of H_{ox}, $H_{ox}H$, $H_{red'}$, and $H_{red'}H$ whose IR signatures are progressively overlapping.[19] Investigating the $H_{ox}/H_{red'}$ redox transition of *Cr*HydA1, we previously explained the observed pH-dependence with a protonation of C417 in $H_{red'}$ (*eq.* C499 in *Cp*I).[19,23] This is not in agreement with the catalytic cycle in Fig. 7. We assume that the pH-dependent decomposition of NaDT caused the apparent shift in $H_{ox}/H_{red'}$ reduction potentials (E^0).[36,52] This is supported by data from Rodríguez-Maciá *et al.* who carefully avoided any NaDT in their preparations of *Cr*HydA1 and did not observe a pH-dependent E^0 for $H_{ox}/H_{red'}$.[21] Additionally, FTIR difference spectra of the $H_{ox}/H_{red'}$ transition show no signals in the SH regime around 2550 cm^{-1} (Fig. S10), which

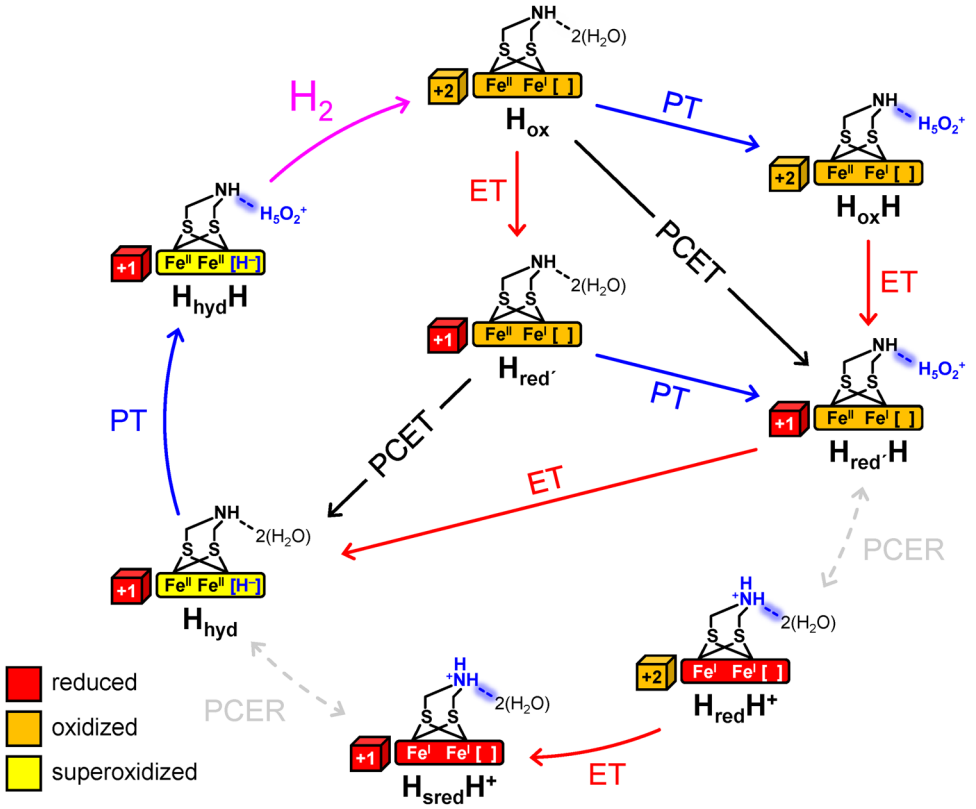

Fig. 7 A proposal of the catalytic cycle involving a Zundel ion in the catalytic PTP. Among all H-cluster species involved, $H_{ox}H$, $H_{red'}H$ and $H_{hyd}H$ represent PTP-protonated intermediates. $[4Fe]_H$ is represented as a cube in the oxidized or reduced state (+2/+1) while the rectangle represents $[2Fe]_H$ in the +4, +3, or +2 states (see legend). For clarity, the CO/CN^- ligands are omitted and only the two water molecules of the catalytic PTP are shown. Proton transfer and electron transfer are denoted as PT and ET, respectively. PCET: proton-coupled electron transfer. PCER: proton-coupled electron rearrangement. Zundel ion: $H_5O_2^+$. See text for further details.

argues against a protonation upon reduction of the H-cluster. The "square scheme" in the first reduction/protonation step in Fig. 7 now reflects these findings.

Afterwards, proton-coupled electronic rearrangement (PCER) prompts electron transfer from $[4Fe]_H$ to $[2Fe]_H$ and proton transfer from W1/W2 to the adt ligand, yielding a NH_2^+ group in the $H_{red}H^+$ state.[15] Then an additional electron reduces $[4Fe]_H^{2+}$ and generates the $H_{sred}H^+$ state. The reason for keeping a deprotonated water molecule in both $H_{red}H^+$ and $H_{sred}H^+$ is based on the experimental observation that no up-shifted $H_{red}H^+$ and $H_{sred}H^+$ states have been reported, even at low pH value.[19] In a second PCER step, the proton migrates toward Fe_d, where it forms a terminal hydride ligand at the expense of the two electrons from $[2Fe]_H$ (H_{hyd}).

The transition from $H_{sred}H^+$ to H_{hyd} might be triggered by protonation of W1/W2 from bulk solvent. Alternatively, H_{hyd} can be formed either *via* an electron transfer step from $H_{red'}H$ or *via* a PCET step from $H_{red'}$.[12,41] As H_{hyd} was observed in the pdt cofactor variant[53] – *i.e.*, independent of adt protonation – we propose a direct conversion *via* $H_{red'}$ or $H_{red'}H$ as the most likely pathway. When the second proton arrives, it first protonates W1/W2, which determines the up-shifted hydride state $H_{hyd}H$. This state was observed *in vivo* previously[12] and identified in *Cr*HydA1-E141D here. The proton from the Zundel ion then migrates toward the hydride-binding H-cluster, H_2 leaves the cofactor and restores the H_{ox} state. The catalytic cycle in Fig. 7 suggests that H-cluster species $H_{ox}H$, $H_{red'}H$, and $H_{hyd}H$ – all of which are accumulated at low pH and under reducing condition – represent transient intermediates determined by a protonation in the proximal section of the PTP, presumably *via* the formation of a Zundel ion.

Conclusions

The present study revisits the formation of the protonated oxidized state of [FeFe]-hydrogenase, $H_{ox}H$. We find that the putative regulatory proton transfer pathway (PTP) is not involved in the formation of $H_{ox}H$ in Group A [FeFe]-hydrogenases from *C. pasteurianum* and *C. reinhardtii*. Site-directed mutagenesis does not affect the accumulation of the $H_{ox}H$ state, although variant *Cp*I-Q195L revealed a potential role of the water molecules around $[4Fe]_H$. During H_2 oxidation, they may serve in redox stabilization. However, our earlier model of a protonated cysteine ligand at $[4Fe]_H$[23–25] must be discarded. Instead, variants targeting the catalytic PTP (*i.e.*, *Cp*I-E279D and *Cr*HydA1-E141D) exhibited a distinctive phenotype, capable of adopting $H_{ox}H$ in the absence of reducing agents. This demonstrates that the formation of the $H_{ox}H$ state is

dependent on the catalytic PTP. We speculate that reductants initiate concerted PCET to facilitate proton delivery toward the protein-bound water cluster in the catalytic PTP, forming a Zundel ion. Quantum mechanical calculations reproduced the IR up-shift that distinguishes H_{ox} from $H_{ox}H$. Accordingly, we propose a catalytic cycle involving the revised $H_{ox}H$ state, indicating that H-cluster species are determined not only by the chemical events occurring in the first and second but also outer coordination sphere effects.[7]

Author contributions

Lingling Liu: investigation, validation, visualization, writing – original draft. Max A. Klamke: validation, writing – original draft. Federica Arrigoni: investigation, validation, visualization, writing – original draft. Oliver Lampret: validation, visualization. Julian Kleinhaus: resources, investigation. Ulf-Peter Apfel: resources, funding acquisition. Eckhard Hofmann: resources, funding acquisition. Claudio Greco: resources, investigation, validation, visualization, funding acquisition, writing – original draft. Thomas Happe: resources, supervision, project administration, funding acquisition, writing – review & editing. Sven T. Stripp: conceptualization, resources, project administration, visualization, funding acquisition, writing – review & editing. Jifu Duan: conceptualization, supervision, project administration, funding acquisition, writing – review & editing.

Conflicts of interest

There are no conflicts to declare.

Data availability

Crystallographic data for CpI-N160L, CpI-Q195L and CpI-N160L-Q195L have been deposited at Protein Data Bank (PDB) under accession numbers 9RJ9, 9RJQ and 9RJO respectively. They can be obtained from following URLs: https://www.rcsb.org/structure/9RJ9, https://www.rcsb.org/structure/9RJQ, https://www.rcsb.org/structure/9RJO. Other data supporting this article have been deposited in Science Data Bank with DOI of https://doi.org/10.57760/sciencedb.31179.

Supplementary information (SI) is available including Methods, additional FTIR spectra, additional structural analyses, cyclic voltammetry data, and further details on the QM calculations. See DOI: https://doi.org/10.1039/d5cp04267d.

Acknowledgements

We thank the Deutsche Forschungsgemeinschaft (DFG; German Research Foundation) for funding (RTG 2341, HA 2555/10-1, 461338801, STR 1554/6-1, and STR 1554/8-1). T. H. additionally thanks the VolkswagenStiftung (Az 98621). U.-P. A. and T. H. were also funded by the DFG under Germany's Excellence Strategy–EXC 2033–390677874– RESOLV. L. L. thanks the China Scholarship Council (CSC) for granting the PhD scholarship. We thank Dr Anna Rovaletti's support in our DFT calculations. Technical support from synchrotron facilities DESY and ESRF during X-ray data collection is appreciated.

References

1 C. Madden, M. D. Vaughn, I. Díez-Pérez, K. A. Brown, P. W. King, D. Gust, A. L. Moore and T. A. Moore, *J. Am. Chem. Soc.*, 2012, **134**, 1577–1582.
2 K. Pandey, S. T. A. Islam, T. Happe and F. A. Armstrong, *Proc. Natl. Acad. Sci. U. S. A.*, 2017, **114**, 3843–3848.
3 Y. Nicolet, C. Piras, P. Legrand, C. E. Hatchikian and J. C. Fontecilla-Camps, *Structure*, 1999, **7**, 13–23.
4 J. W. Peters, W. N. Lanzilotta, B. J. Lemon and L. C. Seefeldt, *Science*, 1998, **282**, 1853–1858.
5 J. Esselborn, N. Muraki, K. Klein, V. Engelbrecht, N. Metzler-Nolte, U.-P. Apfel, E. Hofmann, G. Kurisu and T. Happe, *Chem. Sci.*, 2016, **7**, 959–968.
6 G. Berggren, A. Adamska, C. Lambertz, T. R. Simmons, J. Esselborn, M. Atta, S. Gambarelli, J.-M. Mouesca, E. Reijerse, W. Lubitz, T. Happe, V. Artero and M. Fontecave, *Nature*, 2013, **499**, 66–69.
7 S. T. Stripp, B. R. Duffus, V. Fourmond, C. Léger, S. Leimkühler, S. Hirota, Y. Hu, A. Jasniewski, H. Ogata and M. W. Ribbe, *Chem. Rev.*, 2022, **122**, 11900–11973.
8 S. T. Stripp, *ACS Catal.*, 2021, **11**, 7845–7862.
9 S. D. Fried and S. G. Boxer, *Acc. Chem. Res.*, 2015, **48**, 998–1006.
10 S. Morra, J. Duan, M. Winkler, P. A. Ash, T. Happe and K. A. Vincent, *Dalton Trans.*, 2021, **50**, 12655–12663.
11 J. Duan, A. Hemschemeier, D. J. Burr, S. T. Stripp, E. Hofmann and T. Happe, *Angew. Chem., Int. Ed.*, 2023, **62**, e202216903.
12 L. S. Mészáros, P. Ceccaldi, M. Lorenzi, H. J. Redman, E. Pfitzner, J. Heberle, M. Senger, S. T. Stripp and G. Berggren, *Chem. Sci.*, 2020, **11**, 4608–4617.
13 S. P. J. Albracht, W. Roseboom and E. C. Hatchikian, *J. Biol. Inorg. Chem.*, 2006, **11**, 88–101.
14 E. J. Reijerse, V. Pelmenschikov, J. A. Birrell, C. P. Richers, M. Kaupp, T. B. Rauchfuss, S. P. Cramer and W. Lubitz, *J. Phys. Chem. Lett.*, 2019, **10**, 6794–6799.
15 C. Sommer, A. Adamska-Venkatesh, K. Pawlak, J. A. Birrell, O. Rüdiger, E. J. Reijerse and W. Lubitz, *J. Am. Chem. Soc.*, 2017, **139**, 1440–1443.
16 S. Katz, J. Noth, M. Horch, H. S. Shafaat, T. Happe, P. Hildebrandt and I. Zebger, *Chem. Sci.*, 2016, **7**, 6746–6752.
17 M. Winkler, M. Senger, J. Duan, J. Esselborn, F. Wittkamp, E. Hofmann, U.-P. Apfel, S. T. Stripp and T. Happe, *Nat. Commun.*, 2017, **8**, 16115.
18 A. Adamska, A. Silakov, C. Lambertz, O. Rüdiger, T. Happe, E. Reijerse and W. Lubitz, *Angew. Chem. Int. Ed.*, 2012, **51**, 11458–11462.
19 K. Laun, I. Baranova, J. Duan, L. Kertess, F. Wittkamp, U.-P. Apfel, T. Happe, M. Senger and S. T. Stripp, *Dalton Trans.*, 2021, **50**, 3641–3650.

20 S. Shima, J. A. Birrell, S. T. Stripp, G. Caserta and O. Lenz, *Iron-Sulfur Clusters*, John Wiley & Sons, Ltd, 2025, pp. 489–540.
21 P. Rodríguez-Maciá, N. Breuer, S. DeBeer and J. A. Birrell, *ACS Catal.*, 2020, **10**, 13084–13095.
22 J. A. Birrell, P. Rodríguez-Maciá, E. J. Reijerse, M. A. Martini and W. Lubitz, *Coord. Chem. Rev.*, 2021, **449**, 214191.
23 M. Senger, K. Laun, F. Wittkamp, J. Duan, M. Haumann, T. Happe, M. Winkler, U.-P. Apfel and S. T. Stripp, *Angew. Chem., Int. Ed.*, 2017, **56**, 16503–16506.
24 M. Senger, S. Mebs, J. Duan, O. Shulenina, K. Laun, L. Kertess, F. Wittkamp, U.-P. Apfel, T. Happe, M. Winkler, M. Haumann and S. T. Stripp, *Phys. Chem. Chem. Phys.*, 2018, **20**, 3128–3140.
25 H. Land, M. Senger, G. Berggren and S. T. Stripp, *ACS Catal.*, 2020, **10**, 7069–7086.
26 S. Mebs, R. Kositzki, J. Duan, L. Kertess, M. Senger, F. Wittkamp, U.-P. Apfel, T. Happe, S. T. Stripp, M. Winkler and M. Haumann, *Biochim. Biophys. Acta, Bioenerg.*, 2018, **1859**, 28–41.
27 P. S. Corrigan, J. L. Tirsch and A. Silakov, *J. Am. Chem. Soc.*, 2020, **142**, 12409–12419.
28 M. A. Martini, O. Rüdiger, N. Breuer, B. Nöring, S. DeBeer, P. Rodríguez-Maciá and J. A. Birrell, *J. Am. Chem. Soc.*, 2021, **143**, 18159–18171.
29 M. Senger, J. Duan, M. V. Pavliuk, U.-P. Apfel, M. Haumann and S. T. Stripp, *Inorg. Chem.*, 2022, **61**, 10036–10042.
30 E. Sönmez, N. Kostopoulos, M. Gamache, M. H. Cheah, P. Huang, A. J. Bagnall, D. T. Filmon, I. Voloshyn, T. Happe, M. Senger, N. Plumeré, A. Sekretareva and G. Berggren, *Anal. Chem.*, 2025, **97**, 26393–26403.
31 J. Duan, M. Senger, J. Esselborn, V. Engelbrecht, F. Wittkamp, U.-P. Apfel, E. Hofmann, S. T. Stripp, T. Happe and M. Winkler, *Nat. Commun.*, 2018, **9**, 4726.
32 A. J. Cornish, K. Gärtner, H. Yang, J. W. Peters and E. L. Hegg, *J. Biol. Chem.*, 2011, **286**, 38341–38347.
33 A. J. Cornish, B. Ginovska, A. Thelen, J. C. S. da Silva, T. A. Soares, S. Raugei, M. Dupuis, W. J. Shaw and E. L. Hegg, *Biochemistry*, 2016, **55**, 3165–3173.
34 H. Tai, S. Hirota and S. T. Stripp, *Acc. Chem. Res.*, 2021, **54**, 232–241.
35 A. S. Bingham, P. R. Smith and J. R. Swartz, *Int. J. Hydrogen Energy*, 2012, **37**, 2965–2976.
36 W. J. Lem and M. Wayman, *Can. J. Chem.*, 1970, **48**, 776–781.
37 G. Zundel, *Advances in Chemical Physics*, John Wiley & Sons, Ltd, 1999, pp. 1–217.
38 M. Senger, V. Eichmann, K. Laun, J. Duan, F. Wittkamp, G. Knör, U.-P. Apfel, T. Happe, M. Winkler, J. Heberle and S. T. Stripp, *J. Am. Chem. Soc.*, 2019, **141**, 17394–17403.
39 P. A. Kollman and L. C. Allen, *Chem. Rev.*, 1972, **72**, 283–303.
40 R. E. Hubbard and M. Kamran Haider, in *Encyclopedia of Life Sciences*, John Wiley & Sons, Ltd, Chichester, UK, 2010, p. a0003011.
41 S. Hong and D. Kim, *Proteins: Struct., Funct., Bioinf.*, 2016, **84**, 43–51.
42 R. C. Puthenkalathil and B. Ensing, *J. Phys. Chem. B*, 2022, **126**, 403–411.
43 O. Lampret, J. Duan, E. Hofmann, M. Winkler, F. A. Armstrong and T. Happe, *Proc. Natl. Acad. Sci. U. S. A.*, 2020, **117**, 20520–20529.
44 D. R. Weinberg, C. J. Gagliardi, J. F. Hull, C. F. Murphy, C. A. Kent, B. C. Westlake, A. Paul, D. H. Ess, D. G. McCafferty and T. J. Meyer, *Chem. Rev.*, 2012, **112**, 4016–4093.
45 D. G. Nocera, *J. Am. Chem. Soc.*, 2022, **144**, 1069–1081.
46 S. Hammes-Schiffer, *J. Am. Chem. Soc.*, 2015, **137**, 8860–8871.
47 M. Park, I. Shin, N. J. Singh and K. S. Kim, *J. Phys. Chem. A*, 2007, **111**, 10692–10702.
48 H. Ogata, K. Nishikawa and W. Lubitz, *Nature*, 2015, **520**, 571–574.
49 H. Kwon, J. Basran, J. M. Devos, R. Suardíaz, M. W. van der Kamp, A. J. Mulholland, T. E. Schrader, A. Ostermann, M. P. Blakeley, P. C. E. Moody and E. L. Raven, *Proc. Natl. Acad. Sci. U. S. A.*, 2020, **117**, 6484–6490.
50 T. Bick, P. M. Dominiak and P. Wendler, *BBA Adv.*, 2024, **5**, 100113.
51 J. H. Artz, O. A. Zadvornyy, D. W. Mulder, S. M. Keable, A. E. Cohen, M. W. Ratzloff, S. G. Williams, B. Ginovska, N. Kumar, J. Song, S. E. McPhillips, C. M. Davidson, A. Y. Lyubimov, N. Pence, G. J. Schut, A. K. Jones, S. M. Soltis, M. W. W. Adams, S. Raugei, P. W. King and J. W. Peters, *J. Am. Chem. Soc.*, 2020, **142**, 1227–1235.
52 M. Wayman and W. J. Lem, *Can. J. Chem.*, 1970, **48**, 782–787.
53 A. Depala, M. T. Lachmann, S. Morra, J. A. Birrell and P. Rodríguez-Maciá, *Chem. Commun.*, 2025, **61**, 6178–6181.

